AIAA SciTech
5-9 January 2015, Kissimmee, Florida
AIAA Guidance, Navigation, and Control Conference



# Spacecraft Adaptive Attitude Control with Application to Space Station Free-Flyer Robotic Capture

Jian-Feng Shi,* Steve Ulrich†
*Carleton University, Ottawa, Ontario K1S 5B6, Canada*
Andrew Allen‡
*MacDonald, Dettwiler and Associates Ltd., Brampton, Ontario, L6S 4J3, Canada*



**In this paper, a nonlinear direct adaptive output control methodology is developed to address the problem of spacecraft attitude control under large dynamics uncertainties. The main advantage of the proposed approach over other adaptive approaches for spacecraft attitude control is that it can handle significantly large inertia uncertainties, without requiring any on-line estimation of the unknown moments of inertia. Furthermore, the implementation of the controller does not require a mathematical model of the plant as the control gain adaptation mechanism relies on feedforward signals from an ideal model designed to provide a satisfactory response to the desired attitude commands, as well as on output tracking errors between the uncertain spacecraft and the ideal model. By modeling the spacecraft as a square nonlinear state-space plant through the use of the modified Rodrigues parameters allows the system to satisfy the almost stricly passive conditions, which are required to establish the formal proof of stability. The performance of the new adaptive attitude control approach is illustrated in numerical simulations for both a simple rigid-body rest-to-rest maneuver and a high-fidelity ISS free-flyer robotic capture maneuver.**

## I. Introduction

Spacecraft rendezvous and docking is playing an important role in missions involving autonomous proximity operations, such as automated inspection, maintenance, repair or refurbishing of a malfunctioning satellite, space structure assembly, and space debris removal. Using a robotic arm to capture a target spacecraft for the purpose of docking provides operation flexibility in the mission planning and allows less massive and complex docking interfaces. The idea of using a robotic manipulator to perform a free-flyer capture was initially tested and perfected by the Space Shuttle during operations in which free-flying satellites were captured by the Shuttle Remote Manipulator System (SRMS). These free-flying satellites include the Spartan satellite, the Wake Shield Facility, and the widely-recognized Hubble Space Telescope (HST). Over the years, various free-flyer captures and docking of spacecraft have been performed, ranging from small satellite missions such as the Japan Aerospace Exploration Agency (JAXA) Engineering Test Satellite 7[1] and Boeing's Orbital Express,[2] to large space platform missions such as the HST Servicing Mission[3] and International Space Station (ISS) cargo spacecraft operations.[4] A recent survey by Flores-Abad et al.[5] provides a comprehensive list of free-flyer spacecraft robotic operations.

Free-flyer capture operations are traditionally performed by human crew operator tracking and capturing the free-flyer target vehicle using the manipulator end-effector camera. For the ISS to achieve a capture of a free-flyer cargo vehicle, the Space Station Remote Manipulator System (SSRMS) maneuvers into a free-flyer inner capture box zone where the free-flyer cargo vehicle is waiting approximately 10 meters below the ISS.[6] Once the astronaut operator on the ISS determines the relative motion is acceptable, the free-flyer vehicle

*Ph.D. Student, Department of Mechanical and Aerospace Engineering, 1125 Colonel By Drive. Member AIAA.
†Assistant Professor, Department of Mechanical and Aerospace Engineering, 1125 Colonel By Drive. Senior Member AIAA.
‡Manager, Guidance, Navigation, and Control Department, 9445 Airport Road.

is commanded to a free-drift mode[a] while the SSRMS latching end-effector (LEE) is maneuvered towards a flight releasable grapple fixture (FRGF) or a power and video grapple fixture (PVGF) on the free-flyer so it can capture the vehicle with its three snare cables in the snaring end ring. To date, three types of free-flyer cargo vehicles are making use of this approach; JAXA's H-II Transfer Vehicle, Space Exploration Technologies Corporation's (SpaceX) Dragon Vehicle, and Orbital Science Corporation's Cygnus Vehicle. From a control perspective, the ISS attitude control system must be able to support a free-flyer capture operation by maintaining stable attitude control while the SSRMS captures and repositions the free-flyer cargo spacecraft. This implies that, as stated in the Space Station Program flight rule, the ISS attitude control system must be placed in an attitude hold mode. The ISS utilizes both control moment gyros (CMGs) and reaction control system for attitude control. While the Russian Orbital Segment (ROS) provides propulsive control, the US On-Orbit Segment (USOS) provides non-propulsive control. More specifically, the ROS utilizes a phase-plane based attitude control system and the USOS utilizes a Proportional, Integral and Derivative (PID) attitude control system.[7–9] When the control torque command exceeds CMG torque capability or when CMG momentum is saturated, the USOS can command the RS thrusters to either augment the control command or desaturate the CMGs. However, in the free-flyer capture attitude hold mode, the current flight rule requires all thrusters to be disabled, including CMG desaturation requests.

One of the main challenges inherent to an attitude hold mode during a free-flyer capture operation is related to the interface misalignment between the LEE and the free-flyer GF since higher interface misalignments may generate higher capture loads in the SSRMS and connecting interfaces. The higher capture loading is due to greater motor torque energy applied into the system to enable the rigidization motor to correct the free-flyer interface misalignments between the LEE cam pockets and the GF cam arms during the rigidization operation. As a consequence of a large misalignment, the ISS attitude control system may be required to compensate for higher and unknown external torques using the ISS CMGs.[10] Additionally, time-varying and uncertain mass properties of the free-flyer vehicle poses a significant control challenge, as mass property and time-varuing flexible modes information may not be available to update the ISS attitude control system. As a result, a single controller which can adapt to these uncertainties, i.e., an adaptive controller, is desired.

Another mission scenario which may benefit from an adaptive controller include the upcoming DARPA's Phoenix on-orbit servicing demonstration mission.[b] One of the key characteristics of this mission is to demonstrate the ability of robotic servicer spacecraft to dock and undock with an uncooperative geostationnary satellite, and the ability to harvest components from this satellite in order to assemble a new structure in space. The servicer spacecraft will then be expected to handle various objects of masses and sizes on the same order as its own. Similarly to an ISS robotic capture of a free-flyer cargo vehicle, such tasks involve large uncertainties in the dynamics properties.

Conventional model-based spacecraft attitude control laws require good knowledge of the different physical parameters used in the dynamics model formulation. Typical examples of model-based nonlinear control schemes are those that include a control input torque term that directly counteracts the gyroscopic term of Euler's rotational equation of motion.[11–13] For this reason, it is well known that model-based control approaches may perform inadequately under unknown parameter variations. To address this problem, several indirect adaptive attitude control laws have been proposed to maintain desired closed-loop dynamics in the presence of unknown dynamics properties.[14–24] These adaptive attitude control laws estimate unknown parameters upon which the controller gains are obtained using some design procedure.[25] However, indirect adaptive control nevertheless requires good knowledge of the dynamics model, as explained by Egardt.[26] In addition, the real-time estimation of unknown physical parameters usually require significant computational power. For example, the indirect adaptive control law by Costic et al.[20] incorporates an angular rate-generating filter in the estimation process of the uncertain spacecraft inertia matrix, which is then explicitly employed in the control law. Ahmed et al.[23] present an approach that identifies the inertia matrix in real time and proves that the process is asymptotically stable. Schaub et al.[24] expand upon this approach by also estimating for disturbance inputs. The aforementioned approaches represent the foundation to provide robustness for large-angle spacecraft slewing maneuvers. Alternatively, direct adaptive control techniques, with the controller gains updated directly in response to tracking errors can be used to address the problem of uncertain dynamics parameters. Advantages of direct adaptive approches is that no estimation of the unknown plant parameters is required. However, until the recent developments made by Barkana,[27]

[a] A free-drifting vehicle will have its reaction control system disabled

[b] http://www.darpa.mil/Our˙Work/TTO/Programs/Phoenix.aspx

the stability of direct adaptive techniques to nonlinear and non-stationary dynamics systems could not be guaranteed.

In this context, the main original contribution of this paper is the development of a direct adaptive controller for the attitude control of spacecraft handling large loads of unknown dynamics properties. The resulting nonlinear output feedback direct adaptive control law is developed upon the Simple Adaptive Control (SAC) theory,[28] is based on the modified Rodrigues parameters attitude representation, and copes with dynamics uncertainties (e.g., unknown principal moments of inertia) by time-varying the controller gains in a way to ensure the plant behaves as closely as possible to an ideal model. Contrarily to other attitude representations such as the quaternion or the Rodrigues (Gibbs vector) parameters, the modified Rodrigues parameters form a minimal parametrization and allow rotations of up to $2\pi$. Based on Barkana's recent work,[27] asymptotic stability is guaranteed by making use of Lyapunov's stability theory and LaSalle's invariance principle.

This paper is organized as follows: Section II presents the derivation of the nonlinear state-space model of a rigid spacecraft using the modified Rodrigues parameters. Section III formally defines the model output tracking problem. In Sec. IV, the direct adaptive controller is developed and the error dynamics is obtained, and in Sec. V, the closed-loop stability of the adaptive system is analyzed. A simple rest-to-rest simulation study in Sec. VI demonstrates the performance of the adaptive control system under large dynamics uncertainties. Finally, in Sec. VII, high-fidelity numerical simulation results obtained with the Space Station Portable Operations Training Simulator (SPOTS) facility are reported to demonstrate the increased performance of the developed adaptive control law compared to a PID control law for an ISS free-flyer robotic capture maneuver.

## II. Spacecraft Attitude Dynamics and Kinematics

In this section, a brief review of the attitude dynamics as well as the kinematics equations using the modified Rodrigues parameters (MRP) is given. Then, for convenience, the nonlinear model for spacecraft rotational motion is rewritten as an Euler-Lagrange system and finally, it is formulated as a nonlinear state-space model, which will be used for the adaptive controller development.

In a body-fixed reference frame, the attitude dynamics of a rigid spacecraft are[29]

$$\boldsymbol{J}\dot{\boldsymbol{\omega}} + \boldsymbol{\omega}^{\times}\boldsymbol{J}\boldsymbol{\omega} = \boldsymbol{\tau} \tag{1}$$

where $\boldsymbol{J}$ denotes the spacecraft inertia matrix, $\boldsymbol{\omega}$ is the angular velocity of the rigid body with respect to an inertial frame, and $\boldsymbol{\tau}$ is the control input torque which is assumed to be provided by thruster jets. It is further assumed that the spacecraft body-fixed reference frame is a principal-axis reference frame and such that inertia matrix has the form

$$\boldsymbol{J} = \begin{bmatrix} J_x & 0 & 0 \\ 0 & J_y & 0 \\ 0 & 0 & J_z \end{bmatrix} \tag{2}$$

where $J_x$, $J_y$, and $J_z$ are the principal moments of inertia.

The MRP parameterization is adopted as a rigid body attitude representation, resulting in a minimal, non-singular attitude description. The MRP is obtained by applying a stereographic projection of the attitude quaternion, which is denoted by $\boldsymbol{q}$ and defined as

$$\boldsymbol{q} = \begin{bmatrix} \boldsymbol{\varepsilon} \\ \eta \end{bmatrix} \tag{3}$$

with

$$\boldsymbol{\varepsilon} = \begin{bmatrix} \varepsilon_1 \\ \varepsilon_2 \\ \varepsilon_3 \end{bmatrix} = \hat{\boldsymbol{a}} \sin(\phi/2) \tag{4}$$

and

$$\eta = \cos(\phi/2) \tag{5}$$

where $\hat{\boldsymbol{a}}$ represents the unit vector corresponding to the axis of rotation and $\phi$ is the angle of rotation. The MRP, denoted by $\boldsymbol{\sigma}$, are given by[30,31]

$$\boldsymbol{\sigma} = \frac{\boldsymbol{\varepsilon}}{1+\eta} = \hat{\boldsymbol{a}} \tan(\phi/4) \tag{6}$$

The kinematics equations of motions are described by using the spacecraft angular velocity, as follows[31,32]

$$\dot{\boldsymbol{\sigma}} = \boldsymbol{T}(\boldsymbol{\sigma})\boldsymbol{\omega} \tag{7}$$

where

$$\boldsymbol{T}(\boldsymbol{\sigma}) = \frac{1}{4}\left[\left(1-\boldsymbol{\sigma}^T\boldsymbol{\sigma}\right)\boldsymbol{I}_3 + 2\boldsymbol{\sigma}^\times + 2\boldsymbol{\sigma}\boldsymbol{\sigma}^T\right] \tag{8}$$

In Eq. (8), $\boldsymbol{I}_3$ is the $3 \times 3$ identity matrix and $\boldsymbol{\sigma}^\times$ denotes the skew-symmetric matrix associated with $\boldsymbol{\sigma} = \begin{bmatrix} \sigma_1 & \sigma_2 & \sigma_3 \end{bmatrix}^T$, that is

$$\boldsymbol{\sigma}^\times \equiv \begin{bmatrix} 0 & -\sigma_3 & \sigma_2 \\ \sigma_3 & 0 & -\sigma_1 \\ -\sigma_2 & \sigma_1 & 0 \end{bmatrix} \tag{9}$$

For convenience, Eqs. (1) and (7) are rewritten as an advantageous nonlinear Euler-Lagrange form[14,33,34]

$$\boldsymbol{H}(\boldsymbol{\sigma})\ddot{\boldsymbol{\sigma}} + \boldsymbol{C}(\boldsymbol{\sigma},\dot{\boldsymbol{\sigma}})\dot{\boldsymbol{\sigma}} = \boldsymbol{u} \tag{10}$$

where the matrices $\boldsymbol{H}(\boldsymbol{\sigma})$ and $\boldsymbol{C}(\boldsymbol{\sigma},\dot{\boldsymbol{\sigma}})$, and control input vector $\boldsymbol{u}$ are defined as

$$\boldsymbol{H}(\boldsymbol{\sigma}) \triangleq \boldsymbol{T}^{-T}(\boldsymbol{\sigma})\boldsymbol{J}\boldsymbol{T}^{-1}(\boldsymbol{\sigma}) \tag{11}$$

$$\boldsymbol{C}(\boldsymbol{\sigma},\dot{\boldsymbol{\sigma}}) \triangleq -\boldsymbol{T}^{-T}(\boldsymbol{\sigma})\left[\boldsymbol{J}\boldsymbol{T}^{-1}(\boldsymbol{\sigma})\dot{\boldsymbol{T}}(\boldsymbol{\sigma})\boldsymbol{T}^{-1}(\boldsymbol{\sigma}) + \left(\boldsymbol{J}\boldsymbol{T}^{-1}(\boldsymbol{\sigma})\dot{\boldsymbol{\sigma}}\right)^\times \boldsymbol{T}^{-1}(\boldsymbol{\sigma})\right] \tag{12}$$

$$\boldsymbol{u} \triangleq \boldsymbol{T}^{-T}(\boldsymbol{\sigma})\boldsymbol{\tau} \tag{13}$$

and where

$$\boldsymbol{T}^{-1}(\boldsymbol{\sigma}) = 4\left(1+\boldsymbol{\sigma}^T\boldsymbol{\sigma}\right)^{-2}\left[\left(1-\boldsymbol{\sigma}^T\boldsymbol{\sigma}\right)\boldsymbol{I}_3 - 2\boldsymbol{\sigma}^\times + 2\boldsymbol{\sigma}\boldsymbol{\sigma}^T\right] \tag{14}$$

*Property 3.1*: The matrix $\boldsymbol{H}(\boldsymbol{\sigma})$ is symmetric positive definite.[14]

Assuming that measurements of both the spacecraft attitude and angular rate are available, which may be provided by a Kalman filter,[35] the Euler-Lagrange dynamics model can further be expressed as a nonlinear square state-space formulation

$$\dot{\boldsymbol{x}} = \boldsymbol{A}(\boldsymbol{x},t)\boldsymbol{x} + \boldsymbol{B}(\boldsymbol{x},t)\boldsymbol{u}, \qquad \boldsymbol{y} = \boldsymbol{C}\boldsymbol{x} \tag{15}$$

where, by defining the state vector as $\boldsymbol{x} = \begin{bmatrix} \boldsymbol{\sigma}^T & \dot{\boldsymbol{\sigma}}^T \end{bmatrix}^T$, the system matrices are given by

$$\boldsymbol{A}(\boldsymbol{x},t) = \begin{bmatrix} \boldsymbol{0} & \boldsymbol{I}_3 \\ \boldsymbol{0} & -\boldsymbol{H}^{-1}(\boldsymbol{\sigma})\boldsymbol{C}(\boldsymbol{\sigma},\dot{\boldsymbol{\sigma}}) \end{bmatrix}, \qquad \boldsymbol{B}(\boldsymbol{x},t) = \begin{bmatrix} \boldsymbol{0} \\ \boldsymbol{H}^{-1}(\boldsymbol{\sigma}) \end{bmatrix}, \qquad \boldsymbol{C} = \begin{bmatrix} \alpha\boldsymbol{I}_3 & \boldsymbol{I}_3 \end{bmatrix} \tag{16}$$

such that the scaled-position-and-velocity output is given by

$$\boldsymbol{y} = \alpha\boldsymbol{\sigma} + \dot{\boldsymbol{\sigma}} \tag{17}$$

where $\alpha$ is the scaling factor. This way, the spacecraft orientation can be controlled through the position feedback while the velocity provides beneficial damping effects.

## III. Control Objective

The control objective consists in forcing the closed-loop dynamics to have the following prescribed linear form

$$\dot{\boldsymbol{x}}_m = \boldsymbol{A}_m \boldsymbol{x}_m + \boldsymbol{B}_m \boldsymbol{u}_m, \qquad \boldsymbol{y}_m = \boldsymbol{C}_m \boldsymbol{x}_m \tag{18}$$

with the state vector defined as

$$\boldsymbol{x}_m = \begin{bmatrix} \boldsymbol{\sigma}_m^T & \dot{\boldsymbol{\sigma}}_m^T \end{bmatrix}^T \tag{19}$$

and where the subsript $m$ refers to the ideal model. Specifically, the desired input-output plant response is expressed in terms of the ideal damping ratio $\zeta$ and undamped natural frequency $\omega_n$, as follows

$$\boldsymbol{A}_m = \begin{bmatrix} \boldsymbol{0} & \boldsymbol{I}_3 \\ -\omega_n^2 \boldsymbol{I}_3 & -2\zeta\omega_n \boldsymbol{I}_3 \end{bmatrix}, \qquad \boldsymbol{B}_m = \begin{bmatrix} \boldsymbol{0} \\ \omega_n^2 \boldsymbol{I}_3 \end{bmatrix}, \qquad \boldsymbol{C}_m = \begin{bmatrix} \alpha_m \boldsymbol{I}_3 & \boldsymbol{I}_3 \end{bmatrix} \tag{20}$$

Note that this ideal model only represents the desired, or ideal, input-output closed-loop behavior of the plant, and it is not based on any explicit *a priori* knowledge about the plant parameters. Indeed, the above differential equations only contain kinematic quantities and no system properties such as inertia terms are present. Additionally, the order of the ideal model can be very small in comparison with the plant order.

The above control objective is to be met under the constraints of no knowledge of the spacecraft inertia parameters (i.e., $\boldsymbol{J}$ is unknown). To quantify the control objective, an output tracking error, denoted by $\boldsymbol{e}_y$, is defined

$$\boldsymbol{e}_y \triangleq \boldsymbol{y}_m - \boldsymbol{y} \tag{21}$$

Since $\boldsymbol{J}$ is unknown, the subsequent controller will contain a direct adaptation law that varies in real-time the control gains in response to the tracking error $\boldsymbol{e}_y$, without generating a dynamics parameter estimate.

## IV. Adaptive Control Design

Let consider the following attitude control law

$$\boldsymbol{\tau} = \boldsymbol{T}^T(\boldsymbol{\sigma})\boldsymbol{u} \tag{22}$$

with the control input $\boldsymbol{u}$ corresponding to the Simple Adaptive Control (SAC) algorithm[28]

$$\boldsymbol{u} = \boldsymbol{K}_e(t)\boldsymbol{e}_y + \boldsymbol{K}_x(t)\boldsymbol{x}_m + \boldsymbol{K}_u(t)\boldsymbol{u}_m \tag{23}$$

### IV.A. Adaptation Law

In Eq. (23), $\boldsymbol{K}_e(t)$ is a stabilizing gain, and $\boldsymbol{K}_x(t)$ and $\boldsymbol{K}_u(t)$ are feedforward gains that contribute to bringing the tracking error to zero. The tracking error is used to generate integral adaptive control gains

$$\dot{\boldsymbol{K}}_{Ie}(t) = \boldsymbol{e}_y \boldsymbol{e}_y^T \boldsymbol{\Gamma}_{Ie} \tag{24}$$

$$\dot{\boldsymbol{K}}_{Ix}(t) = \boldsymbol{e}_y \boldsymbol{x}_m^T \boldsymbol{\Gamma}_{Ix} \tag{25}$$

$$\dot{\boldsymbol{K}}_{Iu}(t) = \boldsymbol{e}_y \boldsymbol{u}_m^T \boldsymbol{\Gamma}_{Iu} \tag{26}$$

where $\boldsymbol{\Gamma}_{Ie}$, $\boldsymbol{\Gamma}_{Ix}$, and $\boldsymbol{\Gamma}_{Iu}$ are matrical coefficients that determine the rate of adaptation of the algorithm. Equations (24)-(26) can be written concisely by defining

$$\boldsymbol{K}_I(t) = \begin{bmatrix} \boldsymbol{K}_{Ie}(t) & \boldsymbol{K}_{Ix}(t) & \boldsymbol{K}_{Iu}(t) \end{bmatrix} \tag{27}$$

$$\boldsymbol{r} = \begin{bmatrix} \boldsymbol{e}_y^T & \boldsymbol{x}_m^T & \boldsymbol{u}_m^T \end{bmatrix}^T \tag{28}$$

such that

$$\dot{\boldsymbol{K}}_I(t) = \boldsymbol{e}_y \boldsymbol{r}^T \boldsymbol{\Gamma}_I \tag{29}$$

where $\boldsymbol{\Gamma}_I$ is the resulting adaptation matrix associated with the integral gain $\boldsymbol{K}_I(t)$. Although only the integral adaptive gain $\boldsymbol{K}_I(t)$ is absolutely necessary to guarantee the convergence of the adaptive control system, it is customary to include the adaptive gain $\boldsymbol{K}_P(t)$ as well, to increase the rate of convergence of the adaptive system toward theoretically perfect tracking. Therefore, the adaptive control gains used in Eq. (23) are obtained as

$$\boldsymbol{K}_e(t) = \boldsymbol{K}_{Pe}(t) + \boldsymbol{K}_{Ie}(t) \tag{30}$$

$$\boldsymbol{K}_x(t) = \boldsymbol{K}_{Px}(t) + \boldsymbol{K}_{Ix}(t) \tag{31}$$

$$\boldsymbol{K}_u(t) = \boldsymbol{K}_{Pu}(t) + \boldsymbol{K}_{Iu}(t) \tag{32}$$

where the proportional adaptive control terms are defined similarly to the integral terms

$$\boldsymbol{K}_{Pe}(t) = \boldsymbol{e}_y \boldsymbol{e}_y^T \boldsymbol{\Gamma}_{Pe} \tag{33}$$

$$\boldsymbol{K}_{Px}(t) = \boldsymbol{e}_y \boldsymbol{x}_m^T \boldsymbol{\Gamma}_{Px} \tag{34}$$

$$\boldsymbol{K}_{Pu}(t) = \boldsymbol{e}_y \boldsymbol{u}_m^T \boldsymbol{\Gamma}_{Pu} \tag{35}$$

Let define the proportional gain matrix as

$$\boldsymbol{K}_P(t) = \begin{bmatrix} \boldsymbol{K}_{Pe}(t) & \boldsymbol{K}_{Px}(t) & \boldsymbol{K}_{Pu}(t) \end{bmatrix} = \boldsymbol{e}_y \boldsymbol{r}^T \boldsymbol{\Gamma}_P \tag{36}$$

such that the total adaptive gain, denoted by $\boldsymbol{K}(t)$ can be obtained as

$$\boldsymbol{K}(t) = \boldsymbol{K}_I(t) + \boldsymbol{K}_P(t) \tag{37}$$

Making use of Eq. (37), the attitude control law (22) can be rewritten as

$$\boldsymbol{\tau} = \boldsymbol{T}^T(\boldsymbol{\sigma}) \boldsymbol{K}(t) \boldsymbol{r} \tag{38}$$

### IV.B. Error Dynamics

When the system tracks the ideal model perfectly, i.e. $\boldsymbol{y}_m = \boldsymbol{y}^* = \boldsymbol{C}\boldsymbol{x}^*$, it moves along some bounded ideal state trajectory denoted by $\boldsymbol{x}^*$, such that Eq. (21) can be rewritten as

$$\boldsymbol{e}_y = \boldsymbol{C}\boldsymbol{x}^* - \boldsymbol{C}\boldsymbol{x} = \boldsymbol{C}\boldsymbol{e}_x \tag{39}$$

where $\boldsymbol{e}_x$ denotes the state error defined as

$$\boldsymbol{e}_x \triangleq \boldsymbol{x}^* - \boldsymbol{x} \tag{40}$$

By time-differentiating Eq. (40), and after some algebra, the following differential equation of the state error is obtained

$$\dot{\boldsymbol{e}}_x = \left(\boldsymbol{A} - \boldsymbol{B}\tilde{\boldsymbol{K}}_e \boldsymbol{C}\right) \boldsymbol{e}_x + \left(\boldsymbol{A}^* - \boldsymbol{A}\right) \boldsymbol{x}^* + \left(\boldsymbol{B}^* - \boldsymbol{B}\right) \boldsymbol{u}^* - \boldsymbol{B}\boldsymbol{K}_p(t)\boldsymbol{r} - \boldsymbol{B}\left(\boldsymbol{K}_I(t) - \tilde{\boldsymbol{K}}\right) \boldsymbol{r} \tag{41}$$

where $\tilde{\boldsymbol{K}}$ denotes a fictious constant control gain matrix (unknown and not required for the implementation) given by

$$\tilde{\boldsymbol{K}} = \begin{bmatrix} \tilde{\boldsymbol{K}}_e & \tilde{\boldsymbol{K}}_x & \tilde{\boldsymbol{K}}_u \end{bmatrix} \tag{42}$$

where $\tilde{\boldsymbol{K}}_e$ denotes the ideal stabilizing control gain and $\tilde{\boldsymbol{K}}_x$ and $\tilde{\boldsymbol{K}}_u$ represent the ideal feedforward control gains. The ideal control input, denoted by $\boldsymbol{u}^*$, occurs under a perfect tracking situation defined by $\boldsymbol{e}_y = \boldsymbol{y}_m - \boldsymbol{y} = \boldsymbol{0}$, such that

$$\boldsymbol{u}^* = \tilde{\boldsymbol{K}}_x \boldsymbol{x}_m + \tilde{\boldsymbol{K}}_u \boldsymbol{u}_m \tag{43}$$

## V. Stability

For completeness, preliminary definitions and a theorem that defines under which conditions a nonlinear square system is almost strictly passive (ASP) is reported (see Barkana[27] for more details). Then, based on these definitions and the ASP theorem, a proof which ensures that the nonlinear attitude dynamics of a spacecraft modeled with the modified Rodrigues parameters and with a scaled-position-and-velocity output matrix is ASP, is developed. Finally, making use of the ASP conditions, the closed-loop stability is discussed.

### V.A. Almost Strictly Passive Nonlinear Systems

*Definition 5.1*: Any nonlinear system $\{\boldsymbol{A}(\boldsymbol{x},t), \boldsymbol{B}(\boldsymbol{x},t), \boldsymbol{C}\}$ with the square state-space realization given by Eq. (15) is uniformly strictly minimum-phase if its zero-dynamics is uniformly stable. In other words, there exist two matrices $\boldsymbol{M}(\boldsymbol{x},t)$ and $\boldsymbol{N}(\boldsymbol{x},t)$ satisfying the following relations

$$\boldsymbol{C}\boldsymbol{M}(\boldsymbol{x},t) = \boldsymbol{0} \tag{44}$$

$$\boldsymbol{N}(\boldsymbol{x},t)\boldsymbol{B}(\boldsymbol{x},t) = \boldsymbol{0} \tag{45}$$

$$\boldsymbol{N}(\boldsymbol{x},t)\boldsymbol{M}(\boldsymbol{x},t) = \boldsymbol{I}_{n-m} \tag{46}$$

such that the resulting zero dynamics given by

$$\dot{\boldsymbol{z}} = \left(\dot{\boldsymbol{N}}(\boldsymbol{x},t) + \boldsymbol{N}(\boldsymbol{x},t)\boldsymbol{A}(\boldsymbol{x},t)\right)\boldsymbol{M}(\boldsymbol{x},t)\boldsymbol{z} \tag{47}$$

is uniformly asymptotically stable.

*Definition 5.2*: Any nonlinear system $\{\boldsymbol{A}(\boldsymbol{x},t), \boldsymbol{B}(\boldsymbol{x},t), \boldsymbol{C}\}$ with the square state-space realization given by Eq. (15) is strictly passive if there exist two positive definite symmetric (PDS) matrices $\boldsymbol{P}(\boldsymbol{x},t)$ and $\boldsymbol{Q}(\boldsymbol{x},t)$ such that the following two conditions are simultaneously satisfied

$$\dot{\boldsymbol{P}}(\boldsymbol{x},t) + \boldsymbol{P}(\boldsymbol{x},t)\boldsymbol{A}(\boldsymbol{x},t) + \boldsymbol{A}^T(\boldsymbol{x},t)\boldsymbol{P}(\boldsymbol{x},t) = -\boldsymbol{Q}(\boldsymbol{x},t) \tag{48}$$

$$\boldsymbol{P}(\boldsymbol{x},t)\boldsymbol{B}(\boldsymbol{x},t) = \boldsymbol{C}^T \tag{49}$$

Equation (48) corresponds to the Lyapunov differential equation and shows that a strictly passive system is uniformly asymptotically stable, whereas Eq. (49) shows that

$$\boldsymbol{B}^T(\boldsymbol{x},t)\boldsymbol{P}(\boldsymbol{x},t)\boldsymbol{B}(\boldsymbol{x},t) = \boldsymbol{B}^T(\boldsymbol{x},t)\boldsymbol{C}^T = \boldsymbol{C}\boldsymbol{B}(\boldsymbol{x},t) \tag{50}$$

which implies that the product $\boldsymbol{C}\boldsymbol{B}(\boldsymbol{x},t)$ is PDS. As most real-world systems are not inherently strictly passive, a class of ASP systems can be defined through *Definition 5.3*.

*Definition 5.3*: Any nonlinear system $\{\boldsymbol{A}(\boldsymbol{x},t), \boldsymbol{B}(\boldsymbol{x},t), \boldsymbol{C}\}$ with the square state-space realization given by Eq. (15) is ASP if there exist two PDS matrices $\boldsymbol{P}(\boldsymbol{x},t)$ and $\boldsymbol{Q}(\boldsymbol{x},t)$ and a constant output feedback gain $\tilde{\boldsymbol{K}}_e$ such that the closed-loop system defined by

$$\boldsymbol{A}_C(\boldsymbol{x},t) = \left(\boldsymbol{A}(\boldsymbol{x},t) - \boldsymbol{B}(\boldsymbol{x},t)\tilde{\boldsymbol{K}}_e\boldsymbol{C}\right) \tag{51}$$

simultaneously satisfies the following ASP relations

$$\dot{\boldsymbol{P}}(\boldsymbol{x},t) + \boldsymbol{P}(\boldsymbol{x},t)\boldsymbol{A}_C(\boldsymbol{x},t) + \boldsymbol{A}_C^T(\boldsymbol{x},t)\boldsymbol{P}(\boldsymbol{x},t) = -\boldsymbol{Q}(\boldsymbol{x},t) \tag{52}$$

$$\boldsymbol{P}(\boldsymbol{x},t)\boldsymbol{B}(\boldsymbol{x},t) = \boldsymbol{C}^T \tag{53}$$

*Theorem 5.1*: Any uniformly strictly minimum-phase nonlinear system $\{\boldsymbol{A}(\boldsymbol{x},t), \boldsymbol{B}(\boldsymbol{x},t), \boldsymbol{C}\}$ with the square state-space realization given by Eq. (15), and with the product $\boldsymbol{CB}(\boldsymbol{x},t)$ being PDS is ASP.

*Proof*: See Barkana.[27]

### V.B. ASP Property of Spacecraft Attitude Dynamics

*Theorem 5.2*: The attitude dynamics of a spacecraft modeled with the modified Rodrigues parameters, and represented as a nonlinear state-space system with a scaled-position-and-velocity output matrix is ASP and satisfies the conditions given by Eqs. (52) and (53).

*Proof*: Invoking *Property 3.1*, it can be seen that the product of $\boldsymbol{C}$ and $\boldsymbol{B}(\boldsymbol{x},t)$, both defined in Eq. (16), is PDS

$$\boldsymbol{CB}(\boldsymbol{x},t) = \begin{bmatrix} \alpha \boldsymbol{I}_3 & \boldsymbol{I}_3 \end{bmatrix} \begin{bmatrix} \boldsymbol{0} \\ \boldsymbol{H}^{-1}(\boldsymbol{\sigma}) \end{bmatrix} = \boldsymbol{H}^{-1}(\boldsymbol{\sigma}) > \boldsymbol{0} \tag{54}$$

Moreover, a simple selection of matrices that satisfies Eqs. (44)- (46) is

$$\boldsymbol{M} = \begin{bmatrix} \boldsymbol{I}_3 \\ -\alpha \boldsymbol{I}_3 \end{bmatrix}, \qquad \boldsymbol{N} = \begin{bmatrix} \boldsymbol{I}_3 & \boldsymbol{0} \end{bmatrix} \tag{55}$$

Such that the zero dynamics is

$$\dot{\boldsymbol{z}} = \left(\boldsymbol{N}(\boldsymbol{x},t)\boldsymbol{A}(\boldsymbol{x},t)\right)\boldsymbol{M}(\boldsymbol{x},t)\boldsymbol{z} = -\alpha \boldsymbol{z} \tag{56}$$

which shows that the zero dynamics is stable and that the nonlinear model of the spacecraft attitude dynamics is uniformly minimum-phase. Invoking *Theorem 5.1* completes the proof.

□

### V.C. Stability Analysis

The proof of stability must considers the adaptive system defined by both Eqs. (29) and (41), in order to show the asymptotic convergence of the errors and that the adaptive control gains are bounded. This is demonstrated through the following theorem.

*Theorem 5.3*: The application of the direct adaptive control law to the attitude dynamics of a spacecraft modeled with the modified Rodrigues parameters, and represented as a nonlinear state-space system with a scaled-position-and-velocity output matrix, ensures that all adaptive control gains are bounded under closed-loop operation, and results in asymptotic convergence of the state and output tracking errors, in the sense that

$$\|\boldsymbol{e}_y\| \to \boldsymbol{0} \quad \text{and} \quad \|\boldsymbol{e}_x\| \to \boldsymbol{0} \quad \text{as} \quad t \to \infty$$

*Proof*: Choosing a continuously-differentiable positive-definite quadratic Lyapunov function of the form

$$V = \boldsymbol{e}_x^T \boldsymbol{P}(\boldsymbol{x},t)\boldsymbol{e}_x + tr\left[\left(\boldsymbol{K}_I(t) - \tilde{\boldsymbol{K}}\right)\boldsymbol{\Gamma}_I^{-1}\left(\boldsymbol{K}_I(t) - \tilde{\boldsymbol{K}}\right)^T\right] \tag{57}$$

and making use of *Theorem 5.2*, i.e., using the ASP relations given by Eqs. (52) and (53), results in the following time-derivative of the Lyapunov function

$$\dot{V} = -\boldsymbol{e}_x^T \boldsymbol{Q}(\boldsymbol{x},t)\boldsymbol{e}_x - 2\boldsymbol{e}_x^T \ \boldsymbol{C}^T \boldsymbol{C}\boldsymbol{e}_x \boldsymbol{r}^T \boldsymbol{\Gamma}_P \boldsymbol{r} \tag{58}$$

The Lyapunov derivative $\dot{V}$ in Eq. (58) is uniformly negative definite with respect to $\boldsymbol{e}_x$, but only negative semi-definite with respect to the entire state space $[\boldsymbol{e}_x, \boldsymbol{K}_I(t)]$. Stability of the adaptive system is therefore guaranteed from Lyapunov stability theory, and all state errors (and output errors), as well as adaptive control gains are bounded.

Furthermore, LaSalle's invariance principle for non-autonomous systems[28,36,37] can be used to demonstrate the asymptotic stability of the tracking errors. As demonstrated by Kaufman et al.,[28] for a negative semi-definite Lyapunov derivative of the form (58), all system trajectories are contained within the domain $\Omega_0 = \{[\boldsymbol{e}_x, \boldsymbol{K}_I(t)] | V([\boldsymbol{e}_x, \boldsymbol{K}_I(t)], t) \leq V([\boldsymbol{e}_{x_0}, \boldsymbol{K}_{I_0}(t)], 0)\}$ (where the subscript $\{\}_0$ denotes the initial conditions), and the entire state space $[\boldsymbol{e}_x, \boldsymbol{K}_I(t)]$ ultimately reaches the domain $\Omega_f = \Omega_0 \cap \Omega$, where $\Omega$ denotes the domain defined by the Lyapunov derivative identical to zero. In other words, the state space $[\boldsymbol{e}_x, \boldsymbol{K}_I(t)]$ ultimately reaches the domain defined by $\dot{V}([\boldsymbol{e}_x, \boldsymbol{K}_I(t)], t) \equiv 0$. Because $\dot{V}([\boldsymbol{e}_x, \boldsymbol{K}_I(t)], t)$ is negative definite in $\boldsymbol{e}_x$, the system ends with $\boldsymbol{e}_x \equiv \boldsymbol{0}$. Finally, since $\boldsymbol{e}_x \equiv \boldsymbol{0}$ implies $\boldsymbol{e}_x = \boldsymbol{e}_y = \boldsymbol{0}$, asymptotic stability of the state and output tracking errors is guaranteed.

□

## VI. Rest-to-Rest Simulation Results

To validate the adaptive control law, a three-axis rest-to-rest reorientation maneuver is proposed. This maneuver is defined with the initial conditions on the angular velocity and modified Rodrigues parameters selected as follows

$$\boldsymbol{\omega}_0 = \begin{bmatrix} 0 & 0 & 0 \end{bmatrix}^T \text{ rad/s}$$

$$\boldsymbol{\sigma}_0 = \begin{bmatrix} -0.1 & 0.5 & 1.0 \end{bmatrix}^T$$

The desired attitude parameters are set to zero, which corresponds to a rotation of approximately 193 deg. The principal moments of inertia of the asymmetrical spacecraft are given by[38,39]

$$J_x = 114 \text{ kg} \cdot \text{m}^2 \qquad J_y = 86 \text{ kg} \cdot \text{m}^2 \qquad J_z = 87 \text{ kg} \cdot \text{m}^2$$

and the scaling factor of the output signal, $\alpha$, is set to 1. The simulations consider an external attitude disturbance $\boldsymbol{\tau}_d$ modeled by a first-order Fourier series as[40]

$$\boldsymbol{\tau}_d = \boldsymbol{a}_0 + \boldsymbol{a}_1 \cos(nt) + \boldsymbol{b}_1 \sin(nt)$$

where $n$ is the orbital mean motion and $\mathbf{a}_0$, $\mathbf{a}_1$, and $\mathbf{b}_1$ are the Fourier coefficients given by

$$\boldsymbol{a}_0 = \begin{bmatrix} -4.14 & 10.2 & -5.07 \end{bmatrix}^T \times 10^{-6} \text{ N} \cdot \text{m}$$

$$\boldsymbol{a}_1 = \begin{bmatrix} 6.92 & -9.05 & 3.40 \end{bmatrix}^T \times 10^{-6} \text{ N} \cdot \text{m}$$

$$\boldsymbol{b}_1 = \begin{bmatrix} -8.77 & 1.33 & 7.56 \end{bmatrix}^T \times 10^{-6} \text{ N} \cdot \text{m}$$

This disturbance model is representative of the net torque caused by the atmospheric drag, solar radiation pressure, gravity gradient, and magnetic field, in a 728 km circular Sun-synchronous orbit.[40] The ideal model was designed with $\zeta = 1.0$ and $\omega_n = 0.02$ rad/s. The control parameters of the adaptive algorithm were selected as follows

$$\boldsymbol{\Gamma}_{P_e} = \boldsymbol{\Gamma}_{I_e} = 1e5 \; \boldsymbol{I}_3 \qquad \boldsymbol{\Gamma}_{P_x} = \boldsymbol{\Gamma}_{I_x} = 1e3 \; \boldsymbol{I}_6 \qquad \boldsymbol{\Gamma}_{P_u} = \boldsymbol{\Gamma}_{I_u} = 1e3 \; \boldsymbol{I}_3$$

The integral structure of the adaptive integral gains is computed online using a standard fourth-order Runge-Kutta (ODE4) algorithm evaluated at a sampling frequency of 100 Hz, and all integral adaptive gains were initialized to zero. A plot of the closed-loop modified Rodrigues parameters, angular velocity and control input torques is shown in Fig. 1.

Although the practical purpose of the adaptive controller is to achieve robust performance under large load variations, the strongest demonstration consists in varying the mass properties of the servicer spacecraft. To this end, numerical simulations using a spacecraft with larger principal moments of inertia were performed as a mean to assess the robustness of the proposed controller to parametric uncertainties in the plant. The

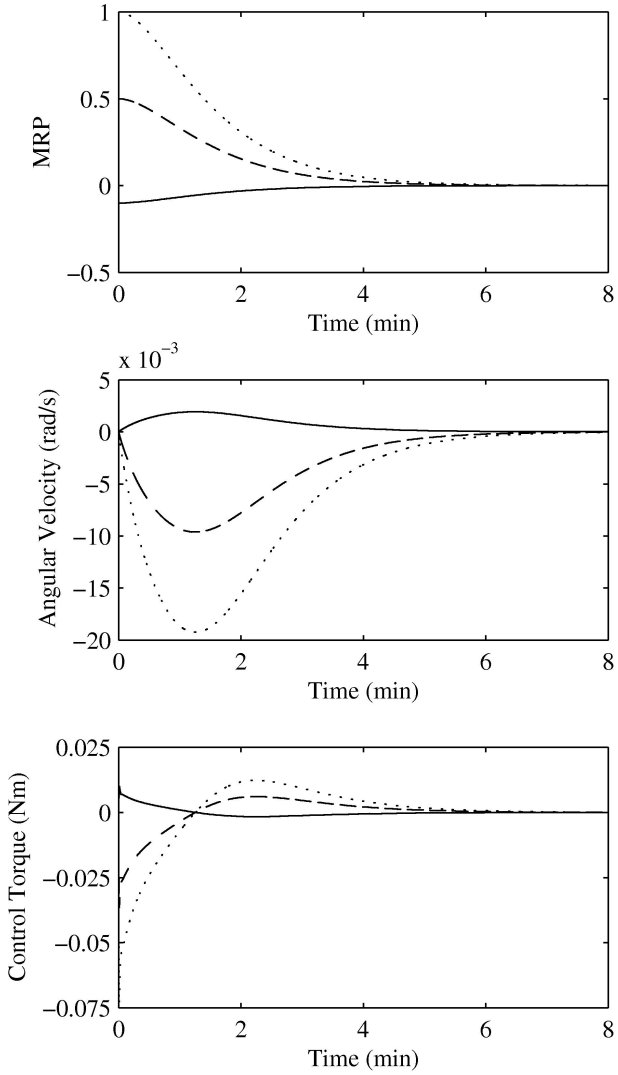


**Figure 1. Three-axis rest-to-rest maneuver with adaptive control. The solid, dashed, and dotted lines correspond to $\{p_1, \omega_x, \tau_x\}$, $\{p_2, \omega_y, \tau_y\}$, and $\{p_3, \omega_z, \tau_z\}$, respectively.**

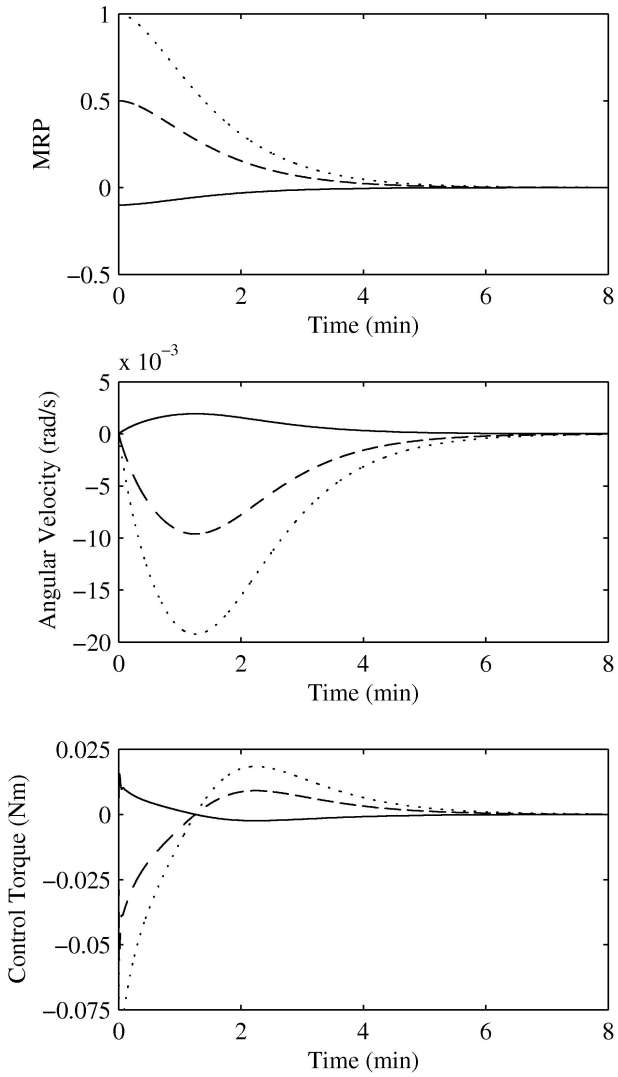


**Figure 2. Three-axis rest-to-rest maneuver with adaptive control in the presence of large inertia uncertainty. The solid, dashed, and dotted lines correspond to $\{p_1, \omega_x, \tau_x\}$, $\{p_2, \omega_y, \tau_y\}$, and $\{p_3, \omega_z, \tau_z\}$, respectively.**

same attitude controller tuned previously with the nominal physical parameters was applied to a spacecraft with principal moments of inertia given by

$$J_x = 171 \ \text{kg} \cdot \text{m}^2 \qquad J_y = 129 \ \text{kg} \cdot \text{m}^2 \qquad J_z = 131 \ \text{kg} \cdot \text{m}^2$$

which represents an uncertainty of 50%. The obtained results are shown in Fig. 2. As shown in this figure, the obtained results are, for all practical purposes, identical to those obtained previously. This desirable behavior of the control system demonstrates that, once the direct adaptive algorithm is properly designed under nominal conditions, the results are not significantly sensitive to uncertainties in the system parameters.

## VII. Space Station Free-Flyer Robotic Capture

This section evaluates the adaptive control method developed in this paper to regulate the ISS attitude during a robotic free-flyer capture. As mentioned earlier, the attitude control system is required to minimize the undesirable ISS attitude motion and attitude bias buildup generated by large interface misalignments, and dynamics parameter uncertainties inherent to a capture maneuver with a free-flyer spacecraft with uncertain moments of inertia. The control methodology was experimentally validated on the MacDonald, Dettwiler and Associates Ltd. (MDA) Space Station Portable Operations Training Simulator (SPOTS), a high-fidelity simulation facility primarily used by the Canadian Space Agency (CSA) to support Mobile Servicing System (MSS) flight software verification, partial operation procedure development and checkout, real-time flight support, end-to-end berthing operations on various ISS robotic operations including module assembly, Orbit Replacement Unit change-outs, manipulator to manipulator payload hand-offs, NASA Robotic Refueling Mission operations, MSS robotic free-space and contact scenarios, and ISS free-flyer captures and releases. Besides the SSP CSA Logistics and Sustaining Engineering program, SPOTS has been used in Space Shuttle program (in aid of the SRMS ASAD dynamics simulator), HST robotic servicing mission design,[41] Orbital Express Demonstration Manipulator System design, Space Infrastructure Servicing design, and Next Generation Canadarm simulator facility. To assist the facility users in visualizing arm and contact motion, several animation tools are also available, one of which is shown in Fig. 3.

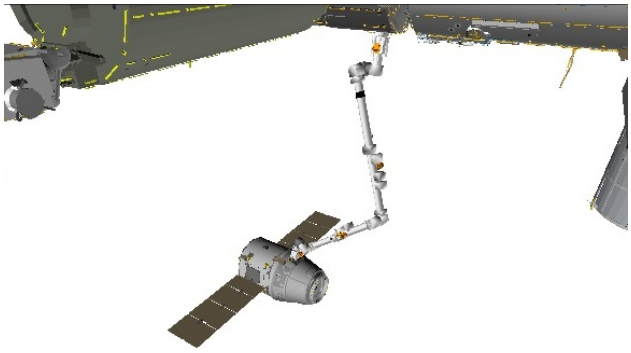

**Figure 3. Visualization of the ISS Dragon free-flyer capture maneuver simulation computed by SPOTS.**

### VII.A. SPOTS Overview

SPOTS models multibody flexible dynamics, orbital mechanics, contact dynamics, encapsulated flight software, and integrated robotic models from CSA, JAXA, NASA, and Roscosmos.[42] In particular, the SSRMS model used in this study is modeled with combining multiple elastic bodies each synthesized with flexible springs calculated from NASA STRucture ANalysis (NASTRAN) finite element models. The link bodies are connected together through a series of one degrees-of-freedom rotational joints. The SSRMS boom structures have the highest number of vibratory modes in comparison with other manipulator links. The SSRMS manipulator joints and motors are modeled to provide realism in joint elasticity and resistive friction. The elastic joint stiffness of the housing and the gear box are represented. The manipulator joint friction is regularly characterized with SSRMS flight data to monitor for joint degradation as well as to maintain an up-to-date calibration of the SPOTS software models. The free-flyer mass properties are simplified for this study demonstration whereas in real operations more precise mass and stiffness matrices are provided by each of the cargo vehicle manufacturers. In the case of the SpaceX's Dragon vehicle, the flexibility of the door that deploys the GF and the solar panels is nevertheless modeled in details.

With SPOTS, contact dynamics is performed by first identifying all contact regions or points and then computing the corresponding contact forces and moments as the result of relative motion and contact of designated bodies. Multiple validations of the SPOTS contact dynamics have been performed, as reported by Ma.[43]

The interface between the LEE and GF, both pictured in Fig. 4, is modeled with snare ring and cables, carriage, and latches. These components are formulated with detailed sets of interacting models representing the snare to GF probe contact, LEE end ring to GF abutment plate and cam arm contact while providing force feedback to the LEE motor modules. A Force and Moment Sensor (FMS) in the LEE assembly is also modeled in the simulator to monitor loads the same way as the actual FMS hardware unit.

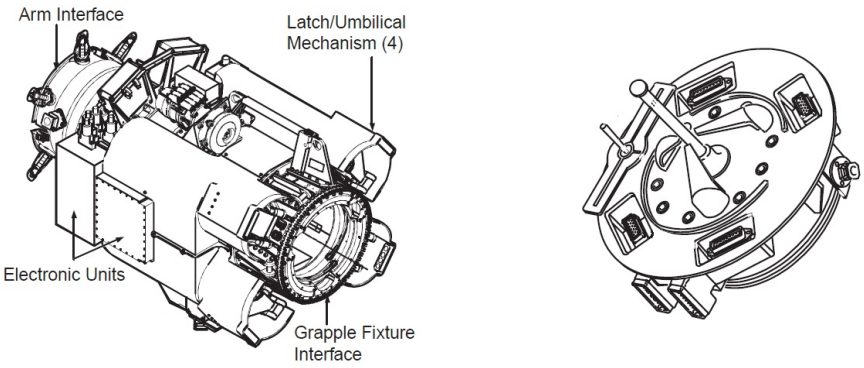


**Figure 4. SSRMS's latching end-effector (left) and grapple fixture (right) (image credit: NASA).**



### VII.B. Controller Implementation Details

As mentioned earlier, the ISS uses its CMGs to stabilize its attitude during a free-flyer robotic capture operation. Indeed, being directly controllable, CMG torque provides the means by which an attitude control law can be implemented. In this study, the total CMG angular momemtum which was limited to 14,642 N·m·s for three operational CMGs,[44] and the torque generated by the CMGs was saturated at 542 N·m per axis.[45]

Since the output of the ISS dynamics in SPOTS is represented by the attitude matrix, a conversion to the MRP attitude representation must be performed. Similar to Rodrigues parameters as described by Hughes,[29] the MRP conversion from an attitude matrix is performed. Let $\boldsymbol{A}_{ISS}$ denote the ISS attitude matrix defined as

$$\boldsymbol{A}_{ISS} = \begin{bmatrix} a_{11} & a_{12} & a_{13} \\ a_{21} & a_{22} & a_{23} \\ a_{31} & a_{32} & a_{33} \end{bmatrix} \tag{59}$$

and let define $\boldsymbol{\Delta}$ as

$$\boldsymbol{\Delta} = \begin{bmatrix} a_{23} - a_{32} \\ a_{31} - a_{13} \\ a_{12} - a_{21} \end{bmatrix} \tag{60}$$

and $\beta$ as

$$\beta = 1 + \text{trace}(\boldsymbol{A}_{ISS}) = 1 + a_{11} + a_{22} + a_{33} \tag{61}$$

such that, if $\beta \neq 0$, the MRPs describing the attitude of the ISS body-fixed reference frame with respect to the inertial reference frame are obtained as

$$\boldsymbol{\sigma}_{ISS} = \frac{\boldsymbol{\Delta}}{\beta \pm 2\sqrt{\beta}} \tag{62}$$

Otherwise, if $\beta = 0$, the MRPs are given by

$$\sigma_{i_{ISS}} = \pm\sqrt{\frac{1 + a_{ii}}{2}}, \ \forall i = 1, 2, 3 \tag{63}$$

### VII.C. Numerical Results

The principal moments of inertia of the 400 metric-ton ISS are given by[46,47]

$$\boldsymbol{J}_{ISS} = \begin{bmatrix} 100 & 0 & 0 \\ 0 & 100 & 0 \\ 0 & 0 & 200 \end{bmatrix} \times 10^6 \ \text{kg} \cdot \text{m}^2$$

The ideal model of the adaptive control scheme was designed with $\zeta = 1.0$ and $\omega_n = 0.02$ rad/s, and the control parameters of the adaptive algorithm were selected as follows

$$\boldsymbol{\Gamma}_{P_e} = \boldsymbol{\Gamma}_{I_e} = 1e17 \ \boldsymbol{I}_3 \qquad \boldsymbol{\Gamma}_{P_x} = \boldsymbol{\Gamma}_{I_x} = 1e3 \ \boldsymbol{I}_6 \qquad \boldsymbol{\Gamma}_{P_u} = \boldsymbol{\Gamma}_{I_u} = 1e9 \ \boldsymbol{I}_3$$

For completeness, the adaptive controller is compared against the ISS PID attitude controller described by[7–9]

$$\boldsymbol{\tau} = \boldsymbol{J}_{ISS} \left[ \boldsymbol{K}_P \boldsymbol{\varepsilon}_e + \boldsymbol{K}_I \int \boldsymbol{\varepsilon}_e + \boldsymbol{K}_D \boldsymbol{\omega}_e \right] \tag{64}$$

where $\boldsymbol{K}_P$, $\boldsymbol{K}_I$ and $\boldsymbol{K}_D$ are the proportional, integral, and derivative gains of the PID controller, and $\boldsymbol{\varepsilon}_e$ and $\boldsymbol{\omega}_e$ are the vector part of the quaternion error and angular velocity command-following error, respectively. According to common ISS practice, the integral control gain $\boldsymbol{K}_I$ is set to zero[9] and both $\boldsymbol{K}_P$ and $\boldsymbol{K}_D$ are selected as

$$\boldsymbol{K}_P = 0.08 \ \boldsymbol{I}_3 \qquad \boldsymbol{K}_D = 0.2 \ \boldsymbol{I}_3$$

The simulation sequence is as follows. Initially, the ISS is at rest and with an attitude of $\begin{bmatrix} 1 & -3 & 0 \end{bmatrix}_{RPY}$ deg, and the GF of free-flyer spacecraft is located $\begin{bmatrix} 14 & 2.1 & 2.1 \end{bmatrix}$ cm from the SSRMS LEE. The initial free-flyer linear and angular relative motion with respect to ISS is set to 33 mm/s and 0.136 deg/s, respectively. This relative motion is tracked by the SSRMS, whose LEE mechanism is setup for a free-flyer capture. Then, at 7.5 seconds into the simulation, the operator triggers the SSRMS hand controller for a capture, which initiates the capture maneuver. Within 60 seconds into the simulation, a full rigidization is achieved and maintained for the duration of the simulation. All the while, the ISS is either in a free-drift mode or in an attitude hold mode (using the benchmark PID controller or the proposed direct attitude control law). The simulation terminates after six minutes into the simulation.

#### *VII.C.1. Test 1: Nominal Conditions*

In this test, both the PID and the adaptive controllers were validated under nominal conditions, i.e., for the conditions under which both controllers' parameters were tuned to provide the best stabilization results. These conditions are defined by a nominal LEE-GF misalignment of $\begin{bmatrix} 5 & 7.1 & 7.1 \end{bmatrix}_{RPY}$ deg, and a free-flyer cargo spacecraft with principal moments of inertia corresponding to those of the axisymmetrical 10 metric-ton Dragon spacecraft depicted in Fig. 5, which are given by[48]

$$\boldsymbol{J}_{Dragon} = \begin{bmatrix} 20 & 0 & 0 \\ 0 & 20 & 0 \\ 0 & 0 & 25 \end{bmatrix} \times 10^3 \ \text{kg} \cdot \text{m}^2$$

Figures 6 to 8 illustrate the ISS orientation devitation from its initial state, the ISS angular velocity, the ISS control torque, and the rigidization force in a free-drift mode, with the PID control law, and with the adaptive control law, respectively. The rigidization force is obtained by a load cell inside the LEE mechanism which measures the resultant load of the cable tensions resolved along the end-effector $x$-axis. The rigidization force is provided as an indicator for time and duration of the cable snare and carriage retraction. Once the rigidization force reaches steady state, the capture process is completed and the SSRMS transitions from limped joints to position hold mode. In the free-drift case, the ISS angular veocity is not stabilized, thus resulting in a steady increase of the attitude errors, which reach 0.47, 0.20 and -0.30 deg five minutes after full rigidization, about the roll, pitch, and yaw axis, respectively. Improvement is of course obtained

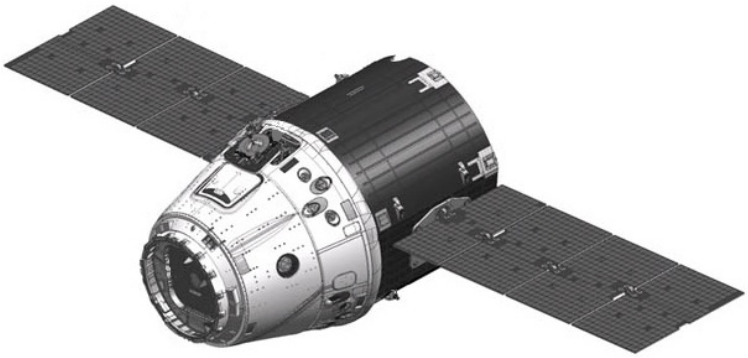

**Figure 5. SpaceX's unmanned Dragon spacecraft (image credit: SpaceX).**



with the PID controller, which regulates both attitude and angular velocity about all three axes within approximately 180 seconds into the simulation. Maximum attitude errors reach $1.42 \times 10^{-3}$, $1.67 \times 10^{-3}$, and $8.96 \times 10^{-4}$ deg about the roll, pitch, and yaw axis, respectively. Finally, further improvements over the PID results are achieved with the proposed adaptive controller, as illustrated in Fig. 8 with both ISS attitude errors and angular velocity being regulated to zero after only 90 seconds into the simulation, with maximum attitude errors of $3.04 \times 10^{-4}$, $2.36 \times 10^{-4}$ and $-2.37 \times 10^{-4}$ deg about the roll, pitch, and yaw axis, respectively. The percentage of CMG momentum capacity is almost identical for both the PID and the adaptive controllers, with maximum capacity of 38.1% and 40.1%, respectively. Therefore, these results indicate that the improvement in attitude stabilization performance achieved with adaptive controller is not obtained at a greater energy demand.

### *VII.C.2. Test 2: Off-Nominal Conditions*

The purpose of this test is to validate the performance of both controllers under dynamics uncertainties. To this end, the same controllers tuned under nominal conditions (defined above) were tested under off-nominal conditions which are defined by a significantly higher LEE-GF misalignment of $\begin{bmatrix} 10 & 10.6 & 10.6 \end{bmatrix}_{RPY}$ deg, and a 20 metric-ton free-flyer cargo spacecraft with inertia matrix given by

$$\boldsymbol{J} = \begin{bmatrix} 40 & 0 & 0 \\ 0 & 40 & 0 \\ 0 & 0 & 50 \end{bmatrix} \times 10^3 \ \text{kg} \cdot \text{m}^2$$

representing an uncertainty of 100% on both the mass and principal moments of inertia. The results are provided in Figs. 9, 10 and 11 for the free-drift, PID, and adaptive control strategy, respectively. As shown in Fig. 10, the tracking performance of the PID control strategy is further aggravated and a maximum overshoot of attitude errors of $2.70 \times 10^{-3}$, $2.71 \times 10^{-3}$, and $-2.01 \times 10^{-3}$ deg about the roll, pitch, and yaw axis, respectively. The attitude errors for the adaptive controller shown in Fig. 11 exhibit maximum peaks of $5.99 \times 10^{-4}$, $-7.35 \times 10^{-4}$, and $-1.04 \times 10^{-3}$ deg about the roll, pitch, and yaw axis, respectively, thus still out-performing the PID controller. Moreover, as in the first test, the adaptive controller stabilizes the attitude to its desired steady state more rapidly than the PID controller. Finally, as before, the percentage of CMG momentum capacity is similar for both the PID and the adaptive controllers, with maximum capacity reaching 72.5% and 72.8%, respectively, which suggest that improved attitude stabilization performance provided by the adaptive controller do not require greater CMG momentum capacity.

## VIII. Conclusion

In this work, based on the simple adaptive control theory, a direct adaptive controller was developed for the attitude control of a rigid spacecraft under dynamics parameter uncertainties. Unlike indirect adaptive attiude controllers, the proposed algorithm does not require the on-line estimation of the unknown parameters. The development was based on the modified Rodrigues parameters attitude parametrization, to model the spacecraft dynamics as a square state-space nonlinear system, to ultimately demonstrate that

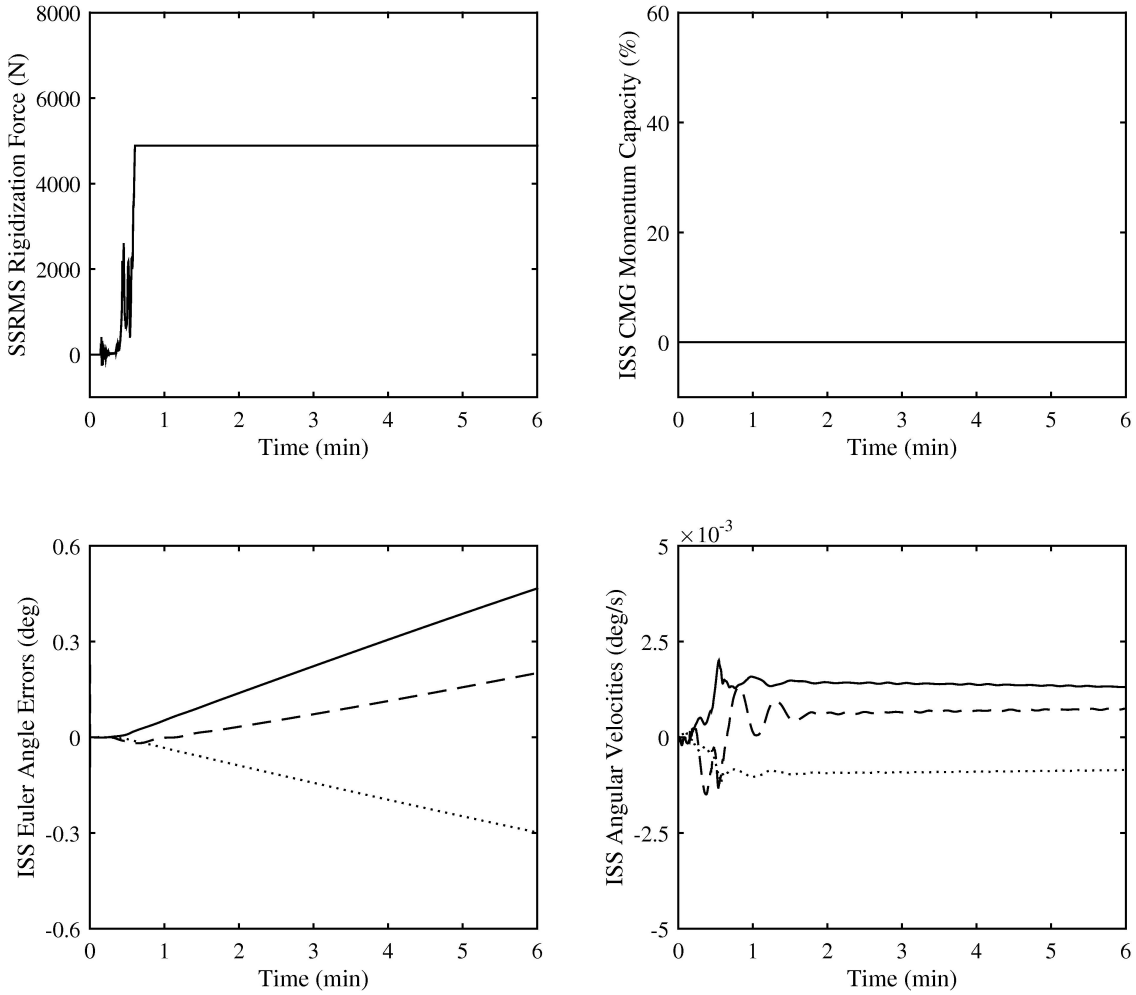


**Figure 6. ISS attitude regulation results under nominal conditions - free-drift mode. The solid, dashed, and dotted lines correspond to {roll, $\omega_x$}, {pitch, $\omega_y$}, and {yaw, $\omega_z$}, respectively.**

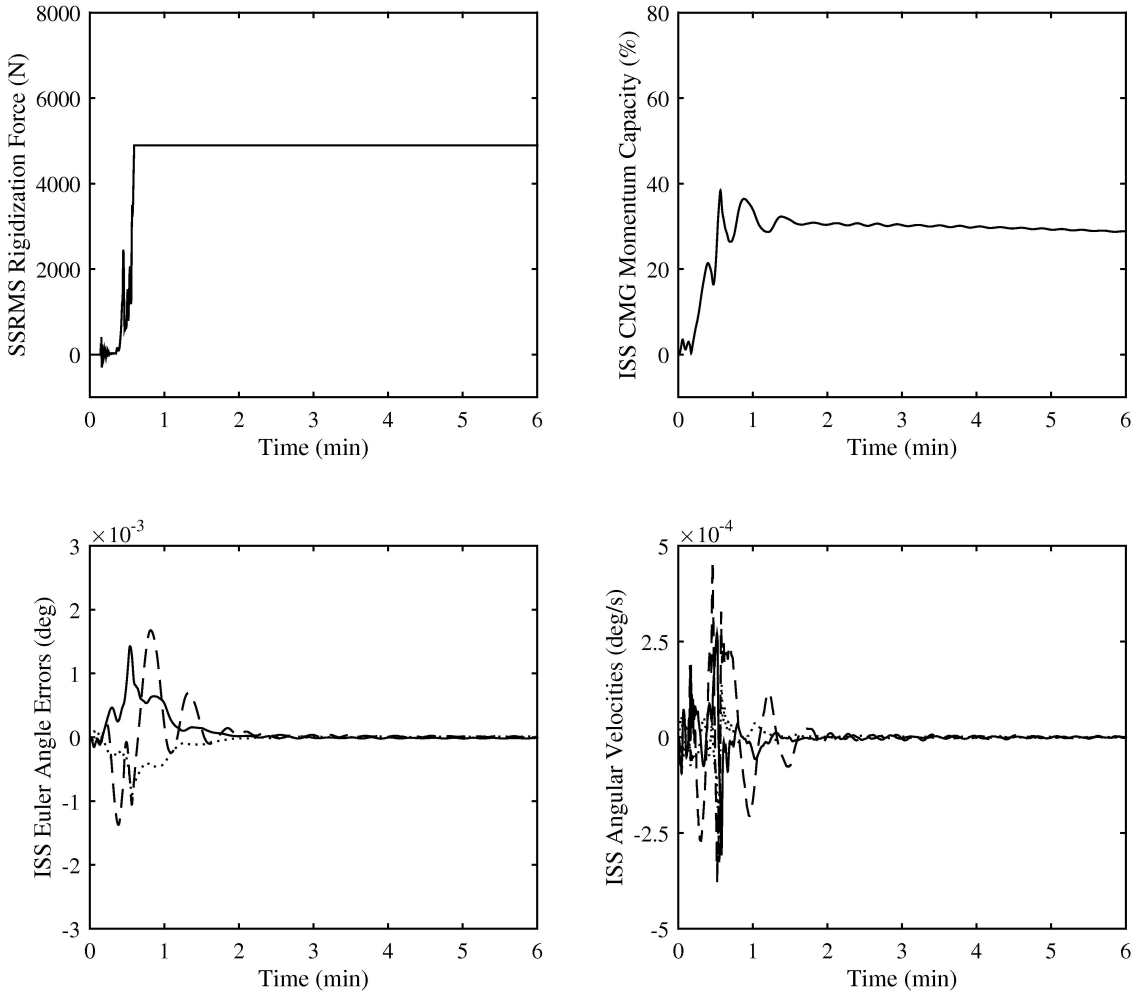


**Figure 7. ISS attitude regulation results under nominal conditions - PID controller. The solid, dashed, and dotted lines correspond to {roll, $\omega_x$}, {pitch, $\omega_y$}, and {yaw, $\omega_z$}, respectively.**

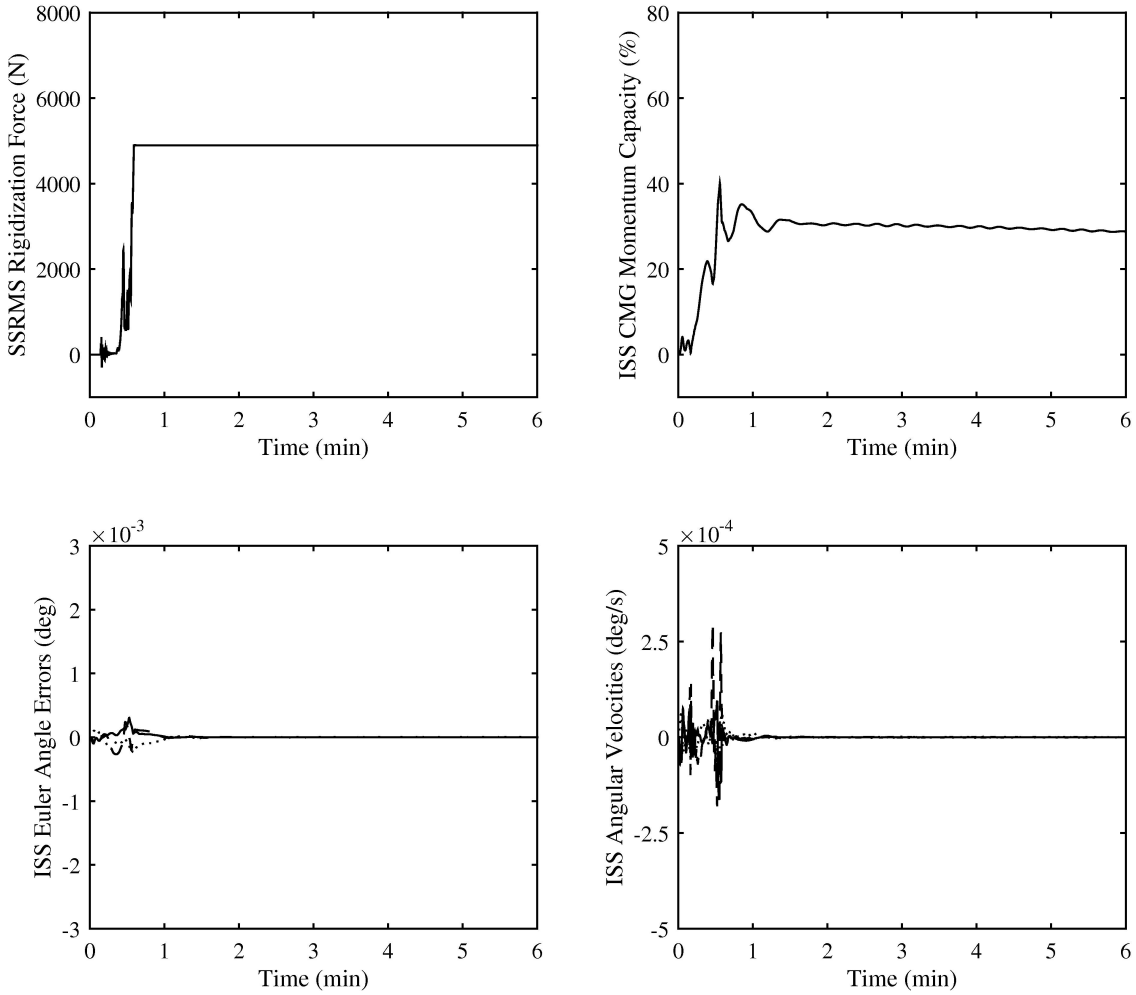


**Figure 8. ISS attitude regulation results under nominal conditions - adaptive controller. The solid, dashed, and dotted lines correspond to {roll, $\omega_x$}, {pitch, $\omega_y$}, and {yaw, $\omega_z$}, respectively.**

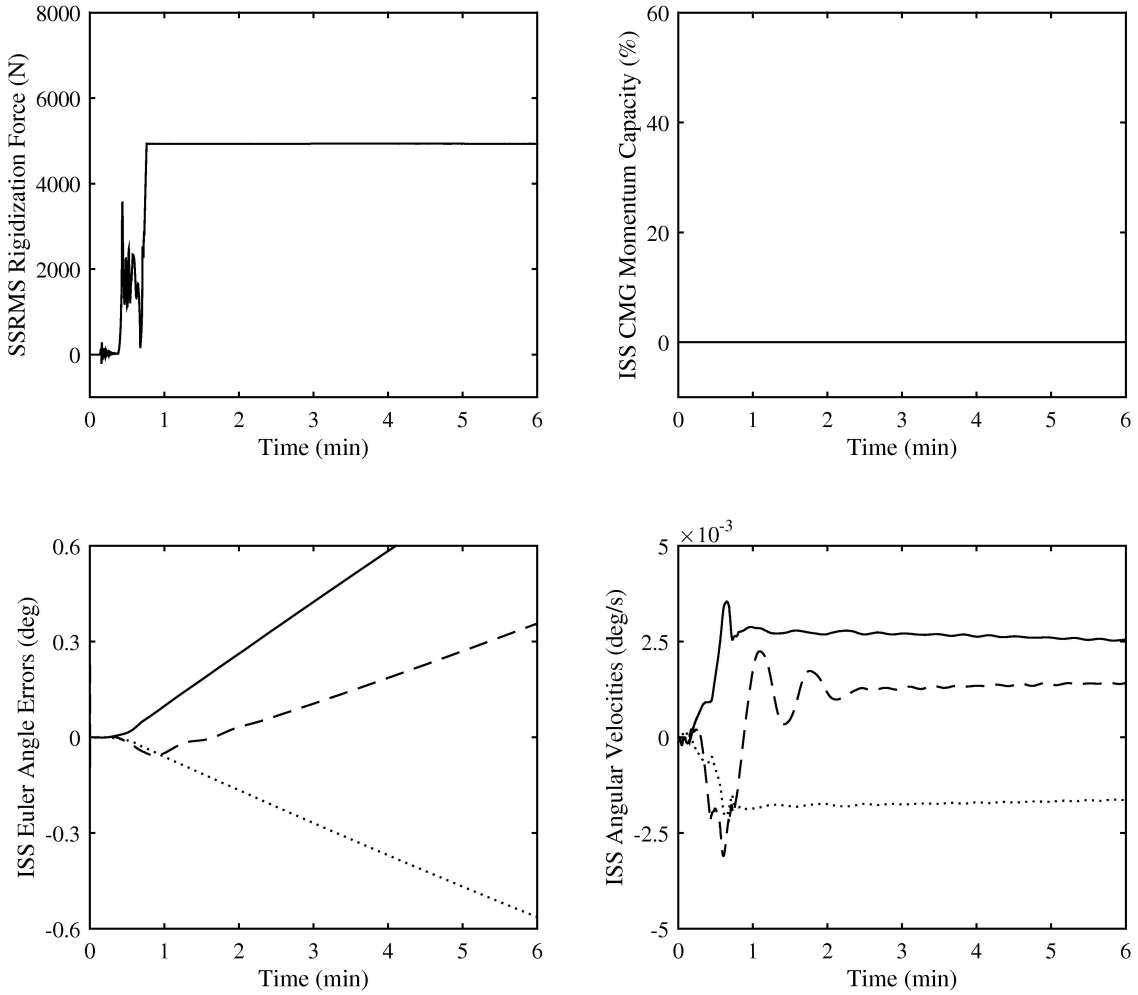


**Figure 9. ISS attitude regulation results under off-nominal conditions - free-drift mode. The solid, dashed, and dotted lines correspond to {roll, $\omega_x$}, {pitch, $\omega_y$}, and {yaw, $\omega_z$}, respectively.**

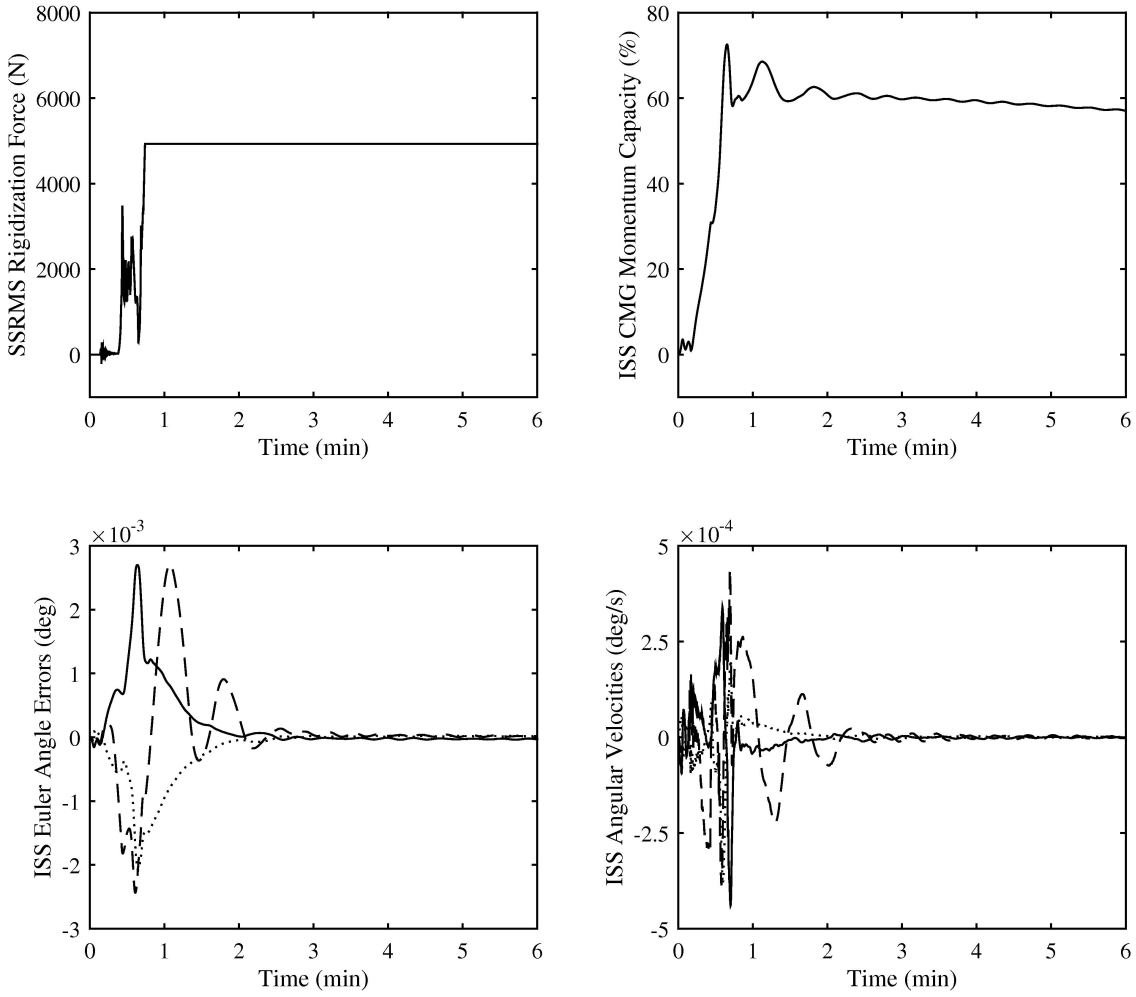


**Figure 10. ISS attitude regulation results under off-nominal conditions - PID controller. The solid, dashed, and dotted lines correspond to {roll, $\omega_x$}, {pitch, $\omega_y$}, and {yaw, $\omega_z$}, respectively.**

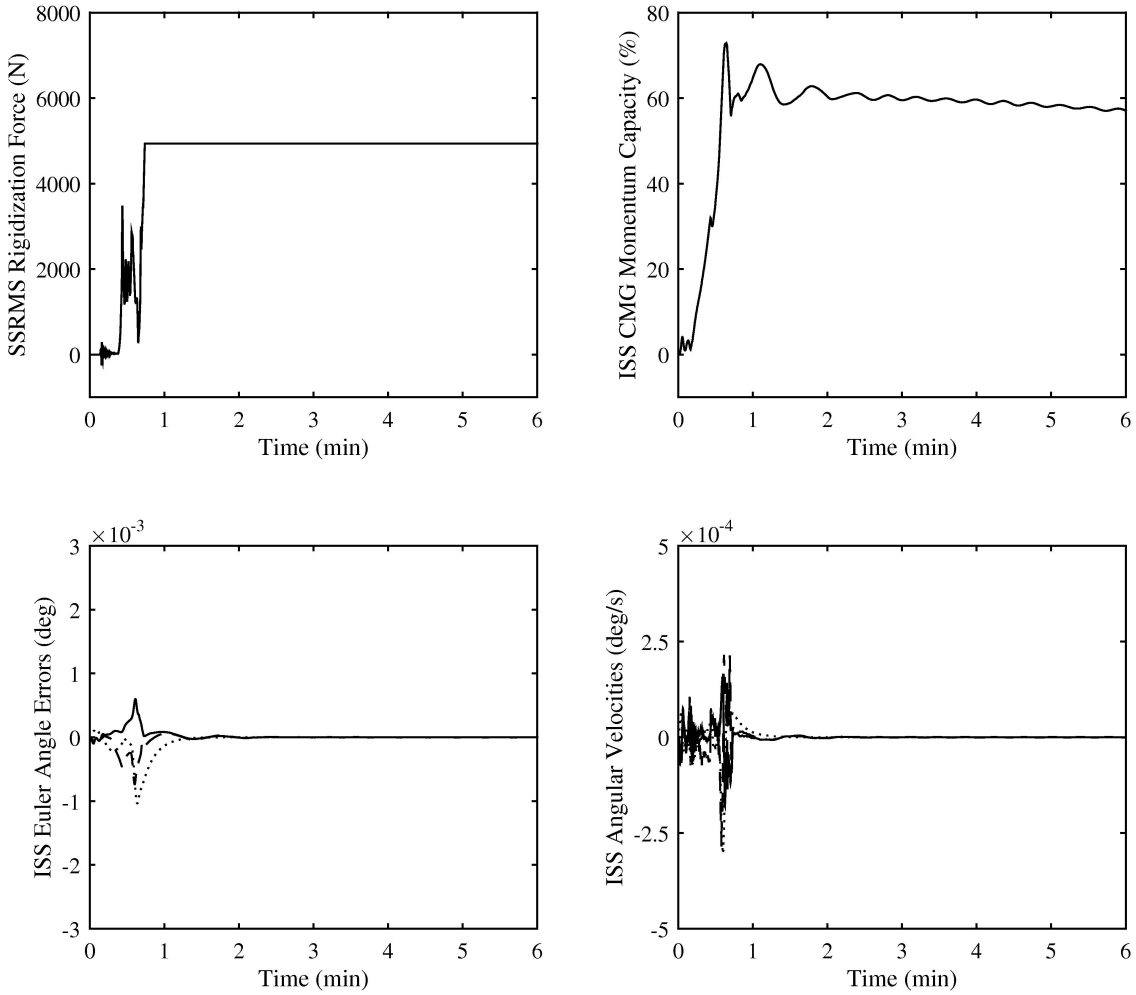


**Figure 11. ISS attitude regulation results under off-nominal conditions - adaptive controller. The solid, dashed, and dotted lines correspond to {roll, $\omega_x$}, {pitch, $\omega_y$}, and {yaw, $\omega_z$}, respectively.**

the resulting attitude dynamics model satisfies the almost strictly passivity conditions, which are required to guarantee the asymptotic stability of the closed-loop nonlinear adaptive control system. Simulation results for a simple rigid-body large rest-to-rest demonstrated a robust attitude control behavior, i.e., a behavior not significantly affected by a large uncertainty in the principal moments of inertia, while results obtained by implementing the adaptive control law into MDA's Space Station Portable Operations Training Simulator for an ISS free-flyer robotic capture scenario suggest that the adaptive algorithm provides improved attitude hold performance compared the actual ISS PID attitude controller, without requiring additional energy demand.

## Acknowledgments

This research was funded by the Natural Sciences and Research Council of Canada's Engage Grant program under the award EGP #469958-14. Financial support from the Canadian Space Agency in the development of the MDA SPOTS facility is also gratefully acknowledged. Finally, the authors acknowledge Kerman Buhariwala and Neil Roger from MDA for their mentorship and inspirations in operating and upgrading the SPOTS facility, as well as valuable discussions and feedback from Itzhak Barkana from Barkana Consulting and Quang M. Lam from LexerdTek Corporation.



## References

[1]Kasai, T., Oda, M., and Suzuki, T., "Results of the ETS-7 Mission Rendezvous Docking and Space Robotics Experiments," *5th International Symposium on Artificial Intelligence, Robotics and Automation in Space*, Noordwijk, The Netherlands, 1999.

[2]Ogilvie, A., Allport, J., Hannah, M., and Lymer, J., "Autonomous Satellite Servicing Using the Orbital Express Demonstration Manipulator System," *9th International Symposium on Artificial Intelligence, Robotics and Automation in Space*, Hollywood, CA, 2008.

[3]Whipple, A., "A Comparison of Human and Robotic Servicing of the Hubble Space Telescope," *NASA Goddard Space Flight Center Systems Engineering Seminar*.

[4]Aziz, S., "Considerations for Next Generation Space Manipulators," *IEEE International Conference on Robotics and Automation*, Piscataway, NJ, 2011.

[5]Flores-Abad, A., Ma, O., Pham, K., and Ulrich, S., "A Review of Space Robotics Technologies for On-orbit Servicing," *Progress in Aerospace Sciences*, Vol. 68, 2014, pp. 1–26.

[6]Smith, C. and Seagram, J., "Free-Flyer Capture - New Robotic Challenges from the International Space Station," *Journal of the British Interplanetary Society*, Vol. 60, 2007, pp. 333–346.

[7]Bedrossian, N., Bhatt, S., Kang, W., and Ross, I. M., "Zero-Propellant Maneuver Guidance," *IEEE Control Systems Magazine*, Vol. 29, No. 5, 2009, pp. 53–73.

[8]Bedrossian, N., Bhatt, S., , Alaniz, A., McCants, E., Nguyen, L., and Chamitoff, G. E., "ISS Contingency Attitude Control Recovery Method for Loss of Automatic Thruster Control," *31st Annual AAS Guidance and Control Conference*, Breckenridge, CO, 2008, AAS Paper 08-001.

[9]Bedrossian, N., Jang, J.-W., Alaniz, A., Johnson, M., Sebelius, K., and Mesfin, Y., "International Space Station US GN&C Attitude Hold Controller Design for Orbiter Repair Maneuver," *AIAA Guidance, Navigation, and Control Conference and Exhibit*, San Fransisco, CA, 2005, AIAA Paper 2005-5853.

[10]Gurrisi, C., Seidel, R., Dickerson, S., Didziulis, S., Frantz, P., and Ferguson, K., "Space Station Control Moment Gyroscope Lessons Learned," *40th Aerospace Mechanisms Symposium*, Space Center, FL, 2010.

[11]Wie, B. and Barba, P., "Quaternion Feedback for Spacecraft Large Angle Maneuvers," *Journal of Guidance, Control, and Dynamics*, Vol. 8, No. 3, 1985, pp. 360–365.

[12]Wie, B., Weiss, H., and Arapostathis, A., "Quaternion Feedback Regulator for Spacecraft Eigenaxis Rotations," *Journal of Guidance, Control, and Dynamics*, Vol. 12, No. 3, 1989, pp. 375–380.

[13]Wie, B. and Lu, J., "Feedback Control Logic for Spacecraft Eigenaxis Rotations Under Slew Rate and Control Constraints," *Journal of Guidance, Control, and Dynamics*, Vol. 18, No. 5, 1995, pp. 375–380.

[14]Slotine, J.-J. E. and Benedetto, M. D. D., "Hamiltonian Adaptive Control of Spacecraft," *IEEE Transactions on Automatic Control*, Vol. 35, No. 7, 1990, pp. 848–852.

[15]Egeland, O. and Godhavn, J.-M., "Passivity-Based Adaptive Attitude Control of a Rigid Spacecraft," *IEEE Transactions on Automatic Control*, Vol. 39, No. 4, 1994, pp. 842–845.

[16]Junkins, J. L., Akella, M. R., and Robinett, R. D., "Nonlinear Adaptive Control of Spacecraft Maneuvers," *Journal of Guidance, Control, and Dynamics*, Vol. 20, No. 6, 1997, pp. 1104–1110.

[17]Cristi, R., Burl, J., and Russo, N., "Adaptive Quaternion Feedback Regulation for Eigenaxis Rotations," *Journal of Guidance, Control, and Dynamics*, Vol. 17, No. 6, 1994, pp. 1287–1291.

[18]Singla, P., Subbarao, K., and Junkins, J. L., "Adaptive Output Feedback Control for Spacecraft Rendezvous and Docking Under Measurement Uncertainty," *Journal of Guidance, Control, and Dynamics*, Vol. 29, No. 4, 2006, pp. 892–902.

[19]Wong, H., de Queiroz, M. S., and Kapila, V., "Adaptive Tracking Control Using Synthesized Velocity from Attitude Measurements," *American Control Conference*, Piscataway, NJ, 2000, pp. 1572–1576.

[20]Costic, B., Dawson, D., de Queiroz, M. S., and Kapila, V., "A Quaternion-Based Adaptive Attitude Tracking Controller Without Velocity Measurements," *IEEE Conference on Decision and Control*, Piscataway, NJ, 2000, pp. 2424–2429.

[21]de Ruiter, A., "Adaptive Spacecraft Attitude Tracking Control with Actuator Saturation," *Journal of Guidance, Control, and Dynamics*, Vol. 33, No. 4, 2010, pp. 1692–1695.

[22]de Ruiter, A., "Spacecraft Attitude Tracking with Guaranteed Performance Bounds," *Journal of Guidance, Control, and Dynamics*, Vol. 36, No. 4, 2013, pp. 1214–1221.

[23]Ahmed, J., Coppola, V. T., and Bernstein, D. S., "Adaptive Asymptotic Tracking of Spacecraft Attitude Motion with Inertia Matrix Identification," *Journal of Guidance, Control, and Dynamics*, Vol. 21, No. 5, 1998, pp. 684–691.

[24]Schaub, H., Akella, M. R., and Junkins, J. L., "Adaptive Control of Nonlinear Attitude Motions Realizing Linear Closed Loop Dynamics," *Journal of Guidance, Control, and Dynamics*, Vol. 24, No. 1, 2001, pp. 95–100.

[25]Narendra, K. S. and Valavani, L. S., "Direct and Indirect Model Reference Adaptive Control," *Automatica*, Vol. 15, No. 6, 1979, pp. 653–664.

[26]Egardt, B., *Stability of Adaptive Controllers*, Springler-Verlag, Berlin, 1979.

[27]Barkana, I., "Output Feedback Stabilizability and Passivity in Nonstationary and Nonlinear Systems," *International Journal of Adaptive Control and Signal Processing*, Vol. 24, No. 7, 2010, pp. 568–591.

[28]Kaufman, H., Barkana, I., and Sobel, K., *Direct Adaptive Control Algorithms: Theory and Applications*, Communications and Control Engineering Series, Springler, New York, NY, 2nd ed., 1997.

[29]Hughes, P. C., *Spacecraft Attitude Dynamics*, John Wiley & Sons, New York, NY, 1986.

[30]Marandi, S. R. and Modi, V. J., "A Preferred Coordinate System and the Associated Orientation Representation in Attitude Dynamics," *Acta Astronautica*, Vol. 15, No. 11, 1987, pp. 833–843.

[31]Schaub, H. and Junkins, J. L., "Stereographic Orientation Parameters for Attitude Dynamics: A Generalization of the Rodrigues Parameters," *The Journal of the Astronautical Sciences*, Vol. 44, No. 1, 1996, pp. 1–19.

[32]Shuster, M. D., "A Survey of Attitude Representations," *The Journal of the Astronautical Sciences*, Vol. 41, No. 3, 1993, pp. 439–517.

[33]Wong, H., de Queiroz, M. S., and Kapila, V., "Adaptive Tracking Control Using Synthesized Velocity from Attitude Measurements," *Automatica*, Vol. 37, No. 6, 2001, pp. 947–953.

[34]Subbarao, K. and Welsh, S., "Nonlinear Control of Motion Synchronization for Satellite Proximity Operations," *Journal of Guidance, Control, and Dynamics*, Vol. 31, No. 5, 2008, pp. 1284–1294.

[35]Crassidis, J. L. and Markley, F. L., "Attitude Estimation Using Modified Rodrigues Parameters," *Flight Mechanics/Estimation Theory Symposium*, Greenbelt, MD, 1996, pp. 71–83.

[36]LaSalle, J., "Stability of Nonautonomous Systems," *Nonlinear Analysis: Theory, Methods, and Applications*, Vol. 1, No. 1, 1981, pp. 83–90.

[37]Barkana, I., "Defending the Beauty of the Invariance Principle," *International Journal of Control*, Vol. 87, No. 1, 2014, pp. 186–206.

[38]III, T. A. W. D. and Sira-Ramirez, H., "Variable Structure Control of Spacecraft Reorientation Maneuvers," *Journal of Guidance, Control, and Dynamics*, Vol. 11, No. 3, 1988, pp. 262–270.

[39]Crassidis, J. L. and Markley, F. L., "Sliding Mode Control Using Modified Rodrigues Parameters," *Journal of Guidance, Control, and Dynamics*, Vol. 19, No. 6, 1996, pp. 1381–1383.

[40]Ulrich, S., Cote, J., and de Lafontaine, J., "In-Flight Attitude Perturbation Estimation for Earth-Orbiting Spacecraft," *The Journal of the Astronautical Sciences*, Vol. 57, No. 3, 2009, pp. 633–665.

[41]Wang, J., Mukherji, R., Ficocelli, M., and Ogilvie, A., "Modeling and Simulation of Robotic System for Servicing Hubble Space Telescope," *IEEE International Conference on Intelligent Robots and Systems*, Piscataway, NJ, 2006, pp. 1026–1031.

[42]Ma, O., Buhariwala, K., Roger, N., Maclean, J., and Carr, R., "MDSF a Generic Development and Simulation Facility for Flexible Complex Robotic Systems," *Robotica*, Vol. 15, No. 1, 1997, pp. 49–62.

[43]Ma, O., "CDT-A General Contact Dynamics Toolkit," *31st International Symposium on Robotics*, Montreal, Canada, 2000, pp. 468–473.

[44]Bedrossian, N., Bhatt, S., Lammers, M., Nguyen, L., and Zhang, Y., "First Ever Flight Demonstration of Zero Propellant Maneuver Attitude Control Concept," *AIAA Guidance, Navigation, and Control Conference and Exhibit*, Hilton Head, SC, 2007, AIAA Paper 2007-6734.

[45]Bedrossian, N. and McCants, E., "Space Station Attitude Control During Payload Operations," *AAS/AIAA Astrodynamics Conference*, Girdwood, AL, 1999, AAS Paper 99-372.

[46]"An Orbiting Laboratory," Tech. Rep. FS-2011-06-011-JSC, NASA Lyndon B. Johnson Space Center, 2011.

[47]Kim, J. W., Crassidis, J. L., Vadali, S. R., and Dershowitz, A. L., "International Space Station Leak Localization Using Attitude Response Data," *Journal of Guidance, Control, and Dynamics*, Vol. 29, No. 5, 2006, pp. 1041–1051.

[48]Couluris, J. and Garvey, T., "SpaceX Mission Operations," *AIAA SpaceOps 2010 Conference*, Huntsville, AL, 2010, AIAA Paper 2010-1937.